PHYSICAL REVIEW B VOLUME 47, NUMBER 19 15 MAY 1993-I

Finite-size effect on the first-order metal-insulator transition in VO_2 films grown by metal-organic chemical-vapor deposition

H. K. Kim,* H. You, R. P. Chiarello, H. L. M. Chang, T. J. Zhang, and D. J. Lam
Materials Science Division, Argonne National Laboratory, Argonne, Illinois 60439
(Received 14 August 1992)

We studied the finite-size effect on the first-order metal-insulator phase transition and the accompanying tetragonal-to-monoclinic structural transition of VO_2 films. The VO_2 films were epitaxially grown by a metal-organic chemical-vapor-deposition technique on the (101) growth plane of a 125-Å-thick TiO_2 buffer layer which was also epitaxially predeposited on polished sapphire $(11\bar{2}0)$ substrates. The thickness of the VO_2 films in this study ranges from 60 to 310 Å. We find that VO_2 films grow isomorphically on the TiO_2 buffer layer resulting in a high degree of epitaxial VO_2 films. We determined structural correlation lengths of the VO_2 films parallel and normal to the growth plane from the x-ray-diffraction widths of VO_2 reflections at room temperature. The structural order parameter associated with the monoclinic distortion and the change in resistivity associated with the metal-insulator phase transition were simultaneously measured using x-ray-diffraction and resistivity measurements. It was found that the transition temperature, width of the transition, and the estimated electronic gap are dependent on the structural correlation length normal to the growth plane. These dependences are discussed in terms of finite-size and substrate effects on the first-order phase transition.

I. INTRODUCTION

Metal oxide systems have unique physical properties, such as metal-insulator phase transitions (MIPT) and the potential for important technological applications.[1] Metal-insulator phase transitions in metal oxide systems have been the subject of intense theoretical[2–6] and experimental[7–15] studies. Several theoretical models[2–6] have been studied and many experimental methods such as optical,[7,8] dielectric,[9] elastic,[10] thermal,[11] and electrical[12,13] measurements have been applied in order to explain the insulating phase, metallic phase, and transition between them. Also, structural studies with neutron[14] and x-ray scattering[15] have focused on the structural phase transformation accompanying MIPT. Despite the similarities in the structural and electronic properties of metal oxide systems, the nature of MIPT can be either first order in some systems such as VO_2 (Ref. 2) or continuous in others such as NbO_2.[14]

The metal-insulator phase transition in bulk VO_2 occurs at $\sim 67\,^\circ$C (Ref. 13) and it is accompanied by a slight structural distortion from a tetragonal rutile structure in the high-temperature metallic phase to a monoclinic structure in the low-temperature insulating phase.[15] In the metallic phase $d_{\parallel}$ and π^* are the lowest-energy bands near the Fermi level and they overlap. In the insulating phase, however, a monoclinic distortion of the lattice by a pairing of the V atoms induces a change in the V-O hybridization, resulting in a rise of the π^* band above the Fermi energy and a splitting of the $d_{\parallel}$ band with one above and the other below the Fermi level. As a result an optical band gap of ~ 0.7 eV between the hybridized π^* state and the lower energy $d_{\parallel}$ state is created. It is also known that the transition to the insulating phase accompanies a charge-density wave formation and condensation of soft modes by the pairing of V atoms, which is based on Peierls instability.[4–6,8] An x-ray scattering study[15] confirmed the existence of a soft phonon mode by measuring diffuse scattering at R points of the Brillouin zone in the metallic phase.

The nature of MIPT of VO_2 is first order. It is not clear why MIPT of VO_2 is first order while that of a similar material NbO_2 is continuous unless a detailed free-energy calculation is performed including all the relevant interactions.[16] In any case the first-order jump in conductivity at the metal-insulator transition temperature (T_c) has been reported to be more than four orders of magnitude for high-quality single-crystal samples.[12]

Despite numerous studies on MIPT of bulk VO_2, studies on VO_2 thin films focused mainly on material aspects such as film quality[17–22] and epitaxial relations to substrates.[23] A number of different methods have been used for VO_2 thin-film preparations: dc sputtering,[17] rf sputtering,[18] reactive ion-beam sputtering,[19] ion-assisted reactive evaporation and annealing,[20] reactive evaporation,[21] dc planar magnetron reactive sputtering,[22] and metal-organic chemical-vapor deposition (MOCVD).[24,25] Some of these studies reported successful deposition of high-quality VO_2 films with a discontinuity of three or four orders of magnitude in conductivity.

In this paper we present a study of the finite-size effects on MIPT of MOCVD grown VO_2 films by simultaneous x-ray diffraction and electrical resistivity measurements.

 ©1993 The American Physical Society

Following this Introduction, experimental details are described in Sec. II. Epitaxial relations of the TiO_2 buffer layer with respect to the substrate and that of VO_2 films with respect to the TiO_2 are described in Sec. III A and the finite-size effects observed in our measurements will be discussed in terms of finite-size scaling theory and substrate effects in Sec. III B. Finally we will draw conclusions in Sec. IV.

II. EXPERIMENT

To achieve a high epitaxial and structural quality, each VO_2 film was epitaxially grown on a TiO_2 buffer layer which is epitaxially predeposited on a sapphire substrate. Titanium dioxide has a tetragonal rutile structure and it has been shown that one can grow it on various crystallographic planes of polished sapphire substrates with a high degree of epitaxy.[24,26] Since the structure of VO_2 at the deposition temperature of 500 °C is also rutile and the lattice constants nearly match with those of TiO_2, we expected the VO_2 films to grow isomorphically on the epitaxial TiO_2 buffer layer and result in high-quality VO_2 epitaxial films.

The MOCVD system is a cold wall, horizontal, open flow system with a rectangular-shaped quartz tube reactor. Titanium isopropoxide [$Ti(OC_3H_7)_4$] and vanadium triethoxide oxide [$VO(OC_2H_5)_3$] were used as metal-organic precursors for TiO_2 and VO_2 deposition, respectively. Pure nitrogen and oxygen were used as carrying gas and oxidant, respectively. Except for deposition time, all other growth parameters were fixed as follows: total gas flow rate, 1300 sccm (standard cubic centimeter per min); pressure, 10 Torr; oxygen flow rate, 200 sccm; metal-organic source temperature, 50 °C; metal-organic source (carrying gas) flow rate, 100 sccm. Growth temperatures were 800 °C for the TiO_2 buffer layer and 500 °C for VO_2 films. A detailed description of the deposition system and sample preparation procedure was presented elsewhere.[23,24]

The x-ray measurements were made with a rotating anode x-ray source and a four-circle diffractometer. The anode target was copper and Cu $K\alpha$ radiation was monochromatized and focused by the (0002) reflection of a vertically bent graphite monochromator. The center of the spectrometer was located at the parafocusing point accepting the incoming beam of $\sim$10 mrad vertically and $\sim$2 mrad horizontally. Additional use of slits allows a range of the longitudinal resolution from 5×10^{-3} to 1×10^{-2} Å^{-1}. Thickness and uniformity, structural phases, crystallinity, and epitaxial orientation of the buffer layer and VO_2 films were characterized by using x-ray reflectivity and diffraction techniques.

The size of the samples was $\sim 5 \times 10$ mm^2. For resistivity measurements two 5-mm-long grooves were made along each 5-mm edge and two bare wires were attached by silver paint into the grooves which are $\sim$8 mm apart. In this way interference of the wires to the incoming and outgoing x ray was minimized. A simple two-probe method was used since the contact resistance between the leads and VO_2 film did not limit our measurements. The temperature was regulated within 0.5°.

For the best VO_2 film quality a deposition time of 10 min was used for TiO_2 buffer layers on a sapphire (11$\bar{2}$0) substrate. It was determined that the TiO_2 (101) plane grows parallel to the substrate surface (11$\bar{2}$0) and the TiO_2 [010] direction is parallel to sapphire [0001] direction as previously found in this system.[25] The 10-min TiO_2 buffer layers were approximately $\sim$ 125 Å thick.

III. RESULTS AND DISCUSSIONS

A. Sample characterization

1. Characterization of the TiO_2 buffer layer

According to previous work,[23–26] TiO_2 films prepared by MOCVD method grow uniformly on the sapphire substrate (11$\bar{2}$0) plane. Since the uniformity of the buffer layer is important to the quality of VO_2 films, we used x-ray reflectivity to find an optimum buffer thickness. In Fig. 1 reflectivity scans for two TiO_2 buffer layers with 10- and 20-min deposition lengths are shown as examples. As we can see the reflectivity for the 20-min film decreases faster with increasing Q than that for the 10-min film. Also a small-amplitude oscillation in the x-ray reflectivity data is visible for the 10-min film. This indicates that the surface of the 10-min film is smoother than that of the 20-min film.[27,28] From the period of the oscillations we estimate the film thickness L of the 10-min TiO_2 film to be $\sim$ 125 Å using $L = 2\pi/\Delta Q$, where ΔQ is the period of oscillation. In addition, the out-of-plane structural correlation length, determined from the width

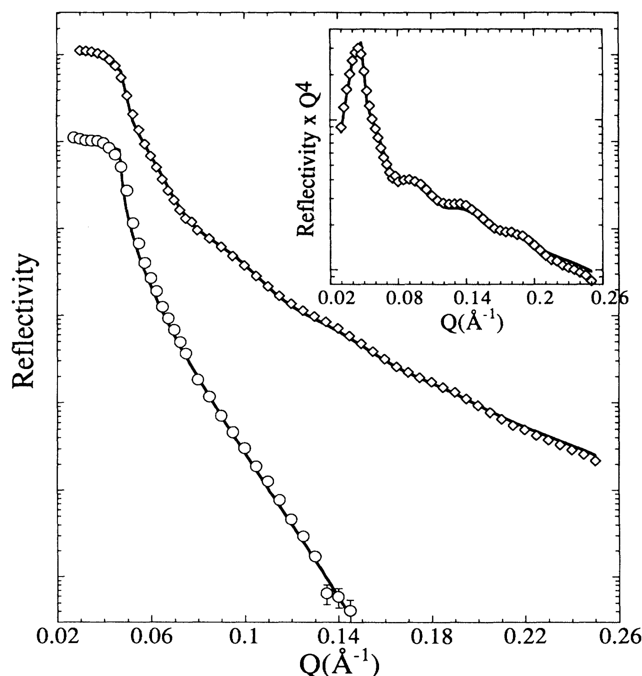

FIG. 1. Reflectivity scan for a 10- and a 20-min deposited TiO_2 buffer layer on sapphire (11$\bar{2}$0). In the inset reflectivity $\times Q^4$ for the 10-min data is shown.

of (101)TiO_2 was also $\sim$ 125 Å indicating that the out-of-plane structural correlation length of the TiO_2 film is nearly equal to the film thickness.

The relevant quantity with respect to studying finite-size effects on MIPT is the out-of-plane correlation length of a sample, not the physical thickness of the film. However, since we find that the correlation length measured from the x-ray scan at (101)TiO_2 and the physical thickness measured from the reflectivity shown in Fig. 1 are the same, we will use the *out-of-plane correlation length* and *thickness* interchangeably in the rest of our discussions. This applies for both the TiO_2 layer and VO_2 films, even though we measure only the out-of-plane correlation length for the VO_2 films.

2. Epitaxy of the VO_2 film with respect to the TiO_2 buffer layer

Figure 2 shows an x-ray scan of a 15-min VO_2 film (15-min VO_2, 10-min TiO_2, sapphire) along the surface normal. Bragg reflections from rutile (101)TiO_2, monoclinic (200)VO_2, and sapphire (11$\bar{2}$0) are indicated in the figure. As mentioned earlier, the transition from a rutile structure to a monoclinic structure is a result of pairing V atoms and a slight distortion from the tetragonal symmetry. Since the distortion angle is small, the positions and the intensities of the rutile reflections in momentum space do not change significantly through the transition. Only weak additional superlattice peaks appear between the reflections. The dimerization of V atoms occurs along the rutile [101] direction and the rutile (101) reflection becomes monoclinic (200) reflection. The occurrence of monoclinic (HKL) reflections with odd integer H signifies the doubling of the unit cell by the dimerization. The rutile and monoclinic reflection indices are related by a transformation matrix given by

$$\begin{pmatrix} H \\ K \\ L \end{pmatrix}_{\text{monoclinic}} = \begin{pmatrix} 0 & 0 & 2 \\ 0 & \bar{1} & 0 \\ 1 & 0 & \bar{1} \end{pmatrix} \begin{pmatrix} H \\ K \\ L \end{pmatrix}_{\text{rutile}} . \qquad (1)$$

Since the structure of TiO_2 is close to that of VO_2 except for a small distortion, the reflections from the TiO_2 rutile structure nearly overlap with the VO_2 monoclinic reflections. In other words, the $(HKL)TiO_2$ reflections are closely positioned to $(2L\ \bar{K}\ H\text{-}L)VO_2$ reflections in reciprocal space. In addition the reciprocal-space position of the sapphire (11$\bar{2}$0) reflection is close to them. Therefore, all three reflections are shown together in Fig. 2. The mosaic spreads measured from the full width at half maximum (FWHM) of rocking curves at the peak positions for the growth planes of TiO_2 and VO_2 films were 0.14° and 0.36°, respectively, as shown in Figs. 3(a) and 3(b), indicating a high degree of epitaxy to the substrate. The in-plane epitaxial relation can be found by ϕ scans at reflections with in-plane momentum components.[25,26] The ϕ scans, circular scans centered at a finite perpendicular momentum transfer and parallel to the surface, are shown in Figs. 3(c) and 3(d). These scans indicate that the (0$\bar{2}$0)TiO_2 and (020)VO_2 planes are well aligned (FWHM = 0.62° for TiO_2 and 1.07° for VO_2) with respect to sapphire (0001) plane indicating a high degree of in-plane epitaxy.

The TiO_2 films are twinned on the sapphire substrate. Since there are two choices for the direction of the (0$\bar{2}$0)TiO_2 reflection on the substrate, there exist two domains randomly occupied in the film. Interestingly it appears that VO_2 grows isomorphically on each of the twin domains of the TiO_2 buffer layer. In other words, the VO_2 film chooses its orientation uniquely to fit the corresponding TiO_2 domain as illustrated in the inset of Fig. 4. In Fig. 4, H scans for the twin domains of TiO_2 (210) and VO_2 (31$\bar{3}$) are shown. By comparing the reflection intensities, the ratio in the domain population is about 5:2 for the two VO_2 domains. As we can see the intensity ratio for the TiO_2 buffer layer is also 5:2. Although we investigated this effect for only one sample, it suggests that the first VO_2 layer senses the stacking direction (see the inset of Fig. 4) of the layer one below the top TiO_2 layer and VO_2 grows into a structure coherent with the underlying TiO_2 rutile structure.

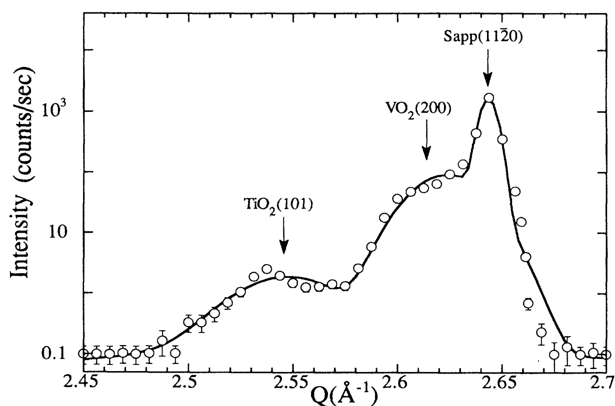

FIG. 2. X-ray scan perpendicular to the growth plane for the 15 min. VO_2, 10 min. TiO_2, sapphire film.

3. Determination of the VO_2 film thickness

We used (31$\bar{3}$) reflection at room temperature for the determination of the out-of-plane correlation and for subsequent temperature-dependent measurements for the following reasons. It is one of the strongest reflections with the odd integer H which are due to doubling of the unit cell below the transition and therefore directly representing the structural correlation of V atom dimerization in the insulating phase. Also, the (31$\bar{3}$) reflection has neither interfering TiO_2 reflections nearby nor higher harmonic contamination ($\lambda/2$) originating from (11$\bar{2}$0)sapphire reflection and (0004) of the graphite monochromator. Some reflections with the odd integer H, such as (100)VO_2 reflection, are subject to the higher harmonic contamination.[29]

First we measure sapphire (3$\bar{1}$2) which is near the position of the (31$\bar{3}$)VO_2 peak to determine the instrumental resolution envelope. The sapphire substrates are single crystals with a sufficiently high quality so that (3$\bar{1}$2) peaks for all substrates are resolution limited.

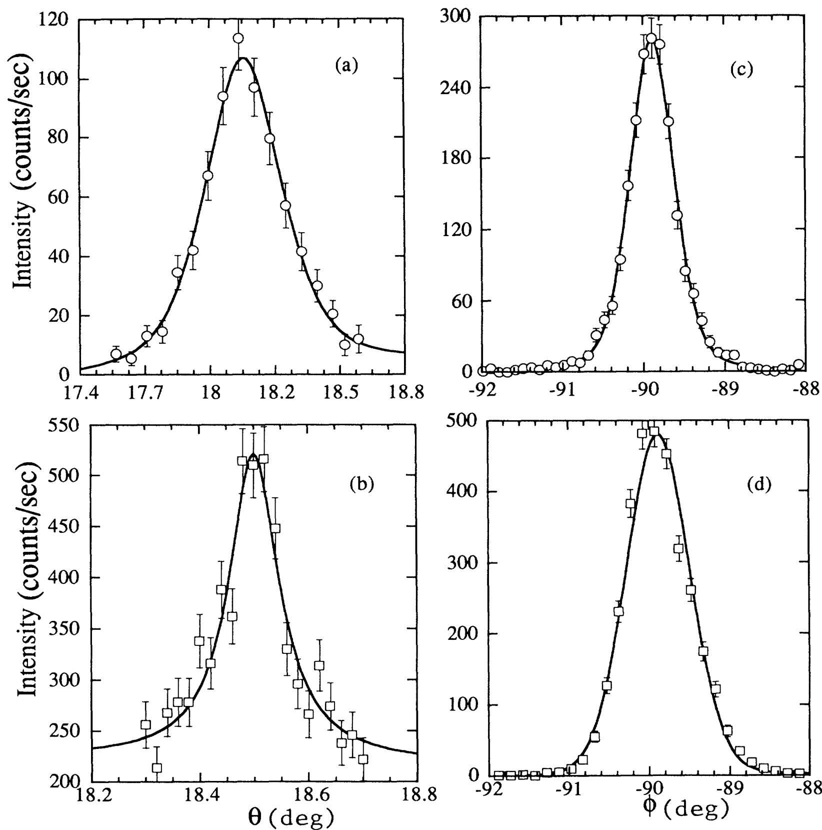

FIG. 3. X-ray-diffraction data of the 15 min. VO_2, 10 min. TiO_2, sapphire film. (a) θ scan of (220)VO_2; (b) θ scan of (121)TiO_2; (c) ϕ scan of (121)TiO_2; (d) ϕ scan of (220)VO_2.

The measured peak profiles of sapphire reflections and the VO_2 reflections were close to a Gaussian functional form. Therefore it was assumed that FWHM(film)^2 = FWHM(measured)$^2-$FWHM(instrumental)^2 to calculate the finite-size broadening of the VO_2 films. Figure 5 shows H scans (out-of-plane direction) of the $(31\bar{3})VO_2$ diffraction plane for the films we studied. We determined that the out-of-plane correlation lengths, or film thickness, were 60, 120, 155, 170, 215, and 310 Å, respectively. The measurements were performed in two separate batches of samples and they are separately shown in Figs. 5(a) and 5(b) since the experimental setups were not identical. The in-plane correlation length was also determined in the same manner from K or L scans of $(31\bar{3})VO_2$. We found that the in-plane correlation length was approximately 500 Å for every sample film that we used in this study.

B. Study of the metal-insulator phase transition

The nature of MIPT of VO_2 involves several different aspects of electronic and structural properties. As mentioned earlier, the Fermi level falls within two degenerate bands, a narrow $d_{\|}$ made of overlapping d orbitals and a broad π^* band made of d orbitals hybridized with p orbitals of oxygen atoms. Because of the difference in the anisotropy, the responses of these two bands to electron-electron correlation (Hubbard-type interaction) or to lattice distortion (Peierls mechanism) are different. Therefore the free energy of this system should include three terms to realistically explain MIPT: (i) free energy of the orbitals; (ii) free energy of spins, which is a key element in Hubbard model; and (iii) free energy of the lattice distortion, which is a key element of Peierls mechanism. One of the main theoretical questions of the VO_2 system was which of the electron-electron correlation or the lattice distortion is the leading term in driving the transition. A complete theoretical study has been carried out to clarify the roles of each contribution to the total

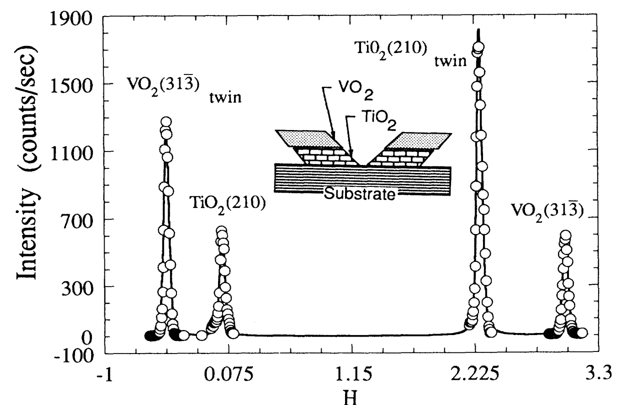

FIG. 4. H scans of the (210)TiO_2 and $(31\bar{3})VO_2$ and their twin counterparts. The inset schematically shows the twin domains of the TiO_2 buffer film and the VO_2 films grown on them.

free energy and a rather clear picture of MIPT has been presented.[16]

According to the theory,[16] the existence of π^* electrons leads the system to undergo a first-order phase transition while the $d_{\parallel}$ band alone would have led the system to undergo a second-order phase transition. The calculated free-energy surface in the local magnetic order-parameter axis and the structural order-parameter axis have two minima separated by a line of maxima. This separation of the two minima results in the first-order phase transition. They also concluded that electron-electron correlation is the primary driving force for MIPT and the lattice distortion follows the primary electronic transition.

The purpose of the simultaneous measurements with resistivity measurements and x-ray diffraction is to learn the finite-size dependence of the band gap (a measure of electronic order parameter) and of structural distortion (structural order parameter). The band-gap energy can be measured from the resistivity and the structural distortion can be measured from the temperature-dependent superlattice peak intensity.

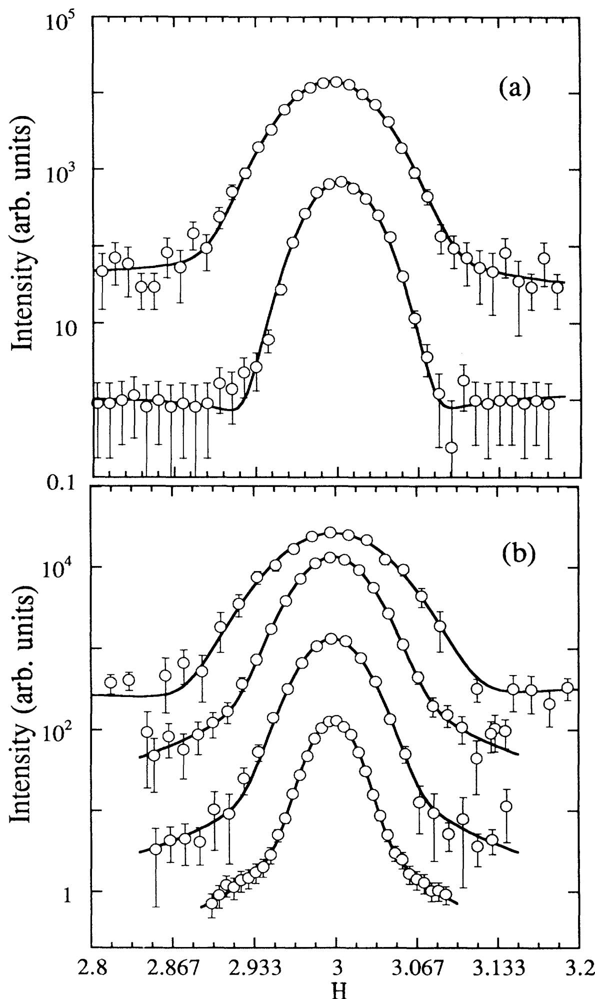

FIG. 5. H scans of VO_2 $(31\bar{3})$ for films of various thickness. The scans shown in (a) and (b) were obtained with different experimental resolutions. The scans were offset for display purpose. The scans from the top are for (a) 310- and 170-Å, and (b) 215-, 155-, 120-, and 60-Å-thick samples, respectively.

The x-ray intensity of the superlattice peak from a lattice distortion can be written in a single phonon approximation with a small-amplitude limit in the following form:

$$I_{\text{superlattice}}(\mathbf{Q}) \approx A(\mathbf{Q})|(\boldsymbol{\eta}_1 + \boldsymbol{\eta}_2) \cdot \mathbf{Q}|^2, \quad (2)$$

where $A(\mathbf{Q})$ is a geometric term and $\boldsymbol{\eta}_1$ and $\boldsymbol{\eta}_2$ are pairing and tilting parameters, respectively. The amplitude of these two distortions is identical, $|\boldsymbol{\eta}_1| = |\boldsymbol{\eta}_2|$, in the case of VO_2, which leads to the monoclinic symmetry ($|\boldsymbol{\eta}_1| \neq |\boldsymbol{\eta}_2|$ leads to a triclinic structure). Since the superlattice reflection intensity is a vector product of $\mathbf{Q}$ and $\boldsymbol{\eta}_1 + \boldsymbol{\eta}_2$, it depends not only on the amplitude of the distortion but also on the polarization of phonon. The $(31\bar{3})VO_2$ diffraction peak is one of the strongest reflection peaks among the superlattice reflections according to Eq. (2).

The conductivity below the transition temperature is proportional to $e^{-E_g/kT}$ since other parameters such as the conduction-band density and mobility of electrons are not sharply dependent on the temperature. Therefore the logarithm of the resistivity is roughly proportional to the size of the gap opening during and below the transition.

Figure 6 shows schematically the behavior of the variation of the band-gap energy and the structural parameter η through MIPT as a function of inverse temperature. They are essentially the reproduction of the figures in the theoretical calculation[16] except for the inversion of the temperature axis. The band-gap energy is indeed at least qualitatively similar to the logarithm of experimentally measured resistivity for bulk samples.[30] The sharp discontinuities in the band-gap energy and the lattice distortion shown in Fig. 6 for a bulk system will become broad and round when the sample size is finite according to the statistical mechanics of finite-size scaling for the first-order phase transition.[31] In the case of an Ising model under a magnetic field, the magnetization curve which would normally show a sharp discontinuity rounds and the susceptibility maximum is linearly proportional to the size of the system.[31] In the case of the VO_2 film samples studied here, only the thickness of the sample needs to be considered finite and it varies from one sample to another. The in-plane correlation lengths measured from H and K scans are substantially larger

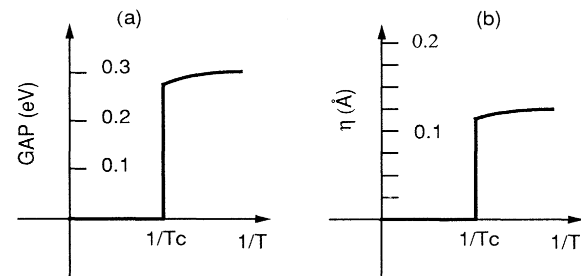

FIG. 6. The theoretically calculated (Ref. 16) band-gap energy and lattice distortion are schematically reproduced.

than the film thickness and change little from one sample to another.

Figure 7 shows a set of data taken for the samples we studied in this work: the logarithm(resistivity) versus inverse temperature in the left-hand-side panels, the integrated intensities of $(31\bar{3})VO_2$ diffraction peak vs inverse temperature in the right-hand-side panels. The integrated intensity for the 60-Å sample is not shown because the intensity of the superlattice reflections were too weak compared with the background to be measured with sufficient counting statistics within a reasonable experimental time scale. The open circles are the data taken in cooling measurements and the filled circles are data taken in heating measurements. The solid lines are fit curves to the data as discussed later. The conductivity (inverse of resistivity) data for 60-, 120-, 215-, and 310-Å-thick samples are presented in one absolute scale for comparison in our previous report.[32] The conductivity for the thickest sample (310 Å) jumps nearly four orders of magnitude at the transition temperature while that for the thinnest sample (60 Å) shows the jump of only two orders of magnitudes.

In both the resistivity and x-ray intensity data of Fig. 7 hysteresis is clearly shown for all samples. The widths of hysteresis do not show any systematic dependence on thickness of the samples. Since hysteresis is due to nucleation barriers of a first-order transition, it is our speculation that the microscopic nature of the substrate affects nucleation sites and in turn affects the width of the hysteresis. Since the width of the hysteresis is identical for x-ray intensity measurements and the resistivity measurements, it shows that the structural and electrical order parameters are closely tied together.

To analyze the data in a systematic fashion, we used an *ad hoc* model of a steplike function,

$$F(T) = \frac{1}{2}\left(a + \frac{b}{T}\right)\left[\tanh\left\{\Delta T\left(\frac{1}{T - T_c}\right)\right\} + 1\right], \quad (3)$$

where $F(T)$ indicates either $\log_{10}(R)$ or $I(31\bar{3})$ and T_c and ΔT are the transition temperature and transition width, respectively. The prefactor $a + \frac{b}{T}$ is to account for the fact that $\ln(R)$ in the insulating phase has a linear dependence on inverse temperature due to the relatively narrow band gap. The parameter b is proportional to the size of the band gap in the insulating phase and $a + \frac{b}{T_c}$ represents the size of the discontinuity at the transition temperature in fitting the $\ln(R)$ data. The width of transition ΔT and transition temperature T_c are shown in Figs. 8(a) and 8(b) and the band-gap energy $E_g = k_B b$ versus the inverse of the sample thickness is shown in Fig. 9.

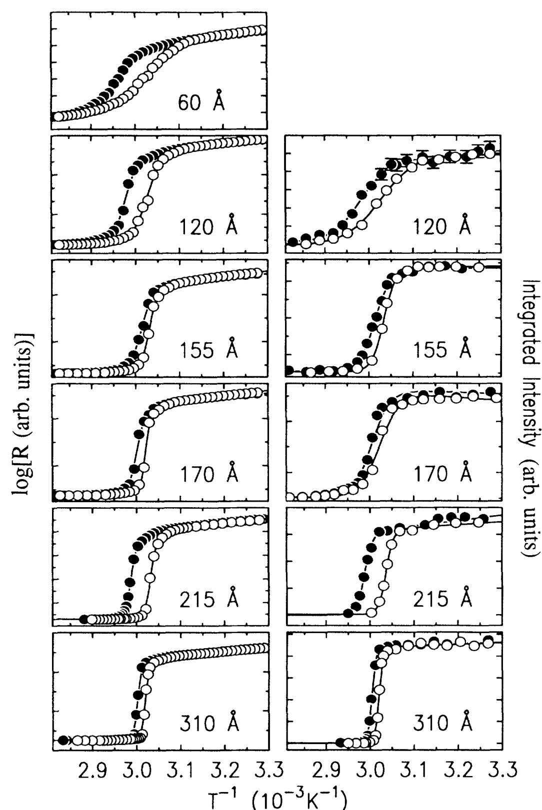

FIG. 7. Temperature dependence of the integrated x-ray-diffraction intensity of $(31\bar{3})$ (right-hand-side panels) and the logarithm of electrical resistivity (left-hand-side panels) for various samples. They are plotted against inverse temperature. The open circles are from cooling experiments and filled circles are from heating experiments. The x-ray data for the 60-Å sample are not available.

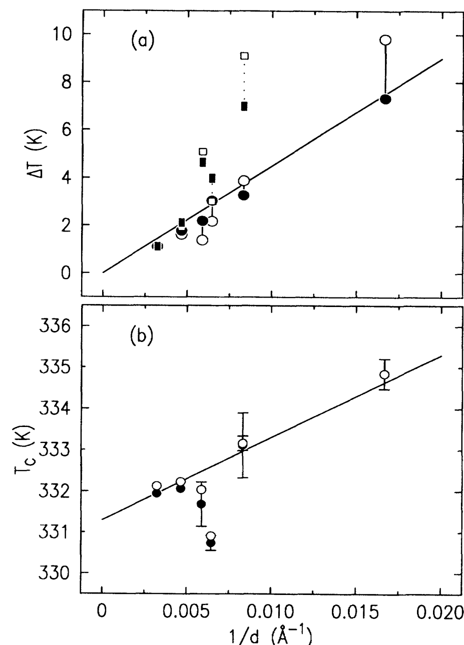

FIG. 8. Sample thickness dependence of (a) transition widths and (b) transition temperatures. (a) The circles are from the resistivity measurements and the squares are from the x-ray measurements. The solid lines are guides to the eye for the transition widths from the resistivity measurements (circles). The open symbols are from the cooling measurements and the filled symbols are from the heating measurements. (b) The open circles are from the resistivity measurements and the filled circles are from the x-ray measurements.

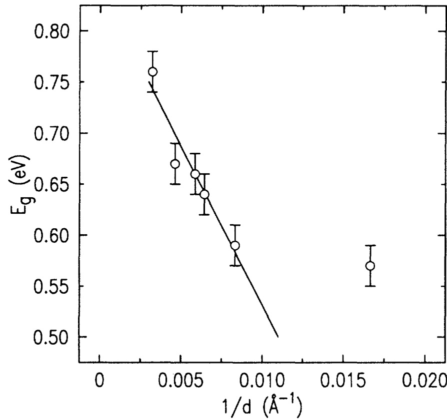

FIG. 9. The band-gap energy of the insulating phase vs sample thickness. The solid line is a guide to the eye.

According to the temperature-dependent finite-size-scaling theory of a first-order phase transition, the deviation from the bulk transition temperature and the width of the transition, the so-called *rounding field*,[33] should scale with the inverse size of the sample,[33–35]

$$T_c(L) - T_c(\infty) \sim 1/L, \quad (4)$$

$$\Delta T(L) \sim 1/L. \quad (5)$$

With these theoretical predictions in mind we will discuss the results shown in Figs. 8(a) and 8(b).

In Fig. 8(a) the transition width ΔT is plotted against the inverse thickness. The circles are from the resistivity measurements and the squares are from the x-ray intensity measurements (open symbols are from the cooling cycle and filled symbols are from the heating cycle). The solid straight line is a guide to the eye for the data points obtained from resistivity (circles). The open and filled circles fall on the straight line quite well. However, the square symbols obtained from 60-, 155-, 170-Å films deviate from the straight line significantly. This observation is also evident from the data in Fig. 7. The width of the transition region in the x-ray intensity measurements appears broader than that in the resistivity measurements for the thin samples. This observation suggests that the electronic correlation length in the system is longer than the structural correlation length for the thin samples. It is probably possible that the development of a long-range order in the unit cell doubling and lattice distortion is disrupted by the influence of the underlying TiO_2 buffer layer. Since the TiO_2 maintains the tetragonal symmetry throughout the transition the strain in the system due to the structural misfit may be significant to the thin samples. The linear dependence of the transition width with respect to the inverse thickness, predicted in the finite-size scaling, seems consistent at least with the resistivity data.

In Fig. 8(b) the transition temperatures, obtained from the x-ray data (filled circles) and from the resistivity data (open circles) by averaging the transition temperatures in the heating and cooling cycles, are shown. It is noticeable that the extrapolation of the transition temperature to the infinitely thick system does not find the transition temperature of the bulk VO_2 (340 K). The suppression of the transition temperature can also be explained by the influence of the TiO_2 buffer layer. Since the TiO_2 buffer layer maintains tetragonal symmetry throughout the transition, the transition temperature can be suppressed to lower the total energy of the system. The fact that the thinner samples have higher transition temperature, despite that the suppression of the transition temperature should be larger on the thinner samples, is not inconsistent with Eq. (4). The deviation of transition temperatures for 155- and 170-Å samples from the solid line also may be from the variation of the substrate quality from one sample to another. A much larger suppression of the transition temperature (~ 20 K) was reported when VO_2 films are sputter grown on MgO substrates,[36] suggesting that the amount of suppression is strongly dependent on the substrate and other growth conditions.

The band-gap energy can in principle be measured from the slope of $\ln(R)$ vs $1/T$ in the insulating phase if it is assumed that the gap energy is constant over the temperature range from which the slope is determined. Therefore, if the gap energy still increases below the transition temperature (in the insulating phase), the value of the gap energy found from the slope of $\ln(R)$ vs $1/T$ will be an overestimation. Nevertheless, the value of gap energy estimated in this manner is displayed in Fig. 9. Since the x-ray intensity does not increase significantly below T_c, as we can see in the right-hand-side panels of Fig. 7, it is a reasonable assumption that the band gap also does not increase. The band-gap energy of the 310-Å sample is close to that of the bulk sample and the band-gap energy decreases linearly with the inverse thickness of the sample except for the 60-Å sample, which shows a large deviation from the solid line (eye guide). Since the x-ray intensity data for the 60-Å sample are not available, we cannot prove that there is a significant increase of the x-ray intensity below the transition temperature. If we assume so, however, the unexpectedly high value of the gap energy for the 60-Å sample can be explained as an overestimation.

IV. CONCLUSIONS

We studied the finite-thickness dependence of the first-order metal-insulator phase transition of VO_2 films whose thickness ranges from 60 to 310 Å. Thermal hysteresis in a transition is observed in simultaneous x-ray diffraction and electrical resistivity measurements for all the samples studied, which is consistent with the first-order nature of phase transition. We find (i) that the transition width (rounding field) measured from the resistivity is linearly dependent on the inverse thickness of the sample as expected from the finite-size-scaling law; (ii) the suppression of T_c, which can be explained by a combined effect of substrates and finite-size scaling; and (iii) that the transition widths measured from the x-ray intensity for the thin samples are broader than those measured from the resistivity, probably due to the influence of the tetragonal

TiO_2 buffer layer. We also find that the gap energy decreases approximately linearly as the thickness of the film decreases. From an experimental point of view, a more systematic sample preparation under a better controlled environment appears essential for more quantitative experimental results. An *in situ* study, although technically difficult, will be the only sure way to avoid preparation-dependent results.

ACKNOWLEDGMENTS

We thank J. Lee for useful discussions. This work was supported by the Division of Materials Sciences, Office of Basic Energy Sciences, U.S. Department of Energy under Contract No. W-31-109-Eng-38. One of us (H.K.K.) was also supported by the Korean Science and Engineering Foundation and RCDAMP.

*Permanent address: Department of Physics, Pusan National University, Pusan, Korea.

[1]See, for example, Kazuhiro Sylvester Goto, *Solid State Electrochemistry and Its Applications to Sensors and Electronic Devices* (Elsevier, New York, 1988).

[2]See, for example, Julius Feinleib and William Paul, Phys. Rev. **155**, 841 (1967); David Adler, Julius Feinleib, Harvey Brooks, and William Paul, *ibid.* **155**, 851 (1967); David Adler and Harvey Brooks, *ibid.* **155**, 826 (1967).

[3]N. F. Mott, Philos. Mag. **6**, 287 (1961); J. Hubbard, Proc. R. Soc. London Ser. A **276**, 238 (1963); **281**, 401 (1964); P. W. Anderson, in *Solid State Physics*, edited by F. Seitz and D. Turnbull (Academic, New York, 1963); D. C. Mattis and W. D. Langer, Phys. Rev. Lett. **25**, 376 (1970).

[4]J. B. Goodenough, Phys. Rev. **120**, 67 (1960); J. Phys. Chem. Solids **6**, 287 (1958).

[5]M. Gupta, A. J. Freeman, and D. E. Ellis, Phys. Rev. B **16**, 3338 (1977).

[6]F. Gervais and W. Press, Phys. Rev. B **31**, 4809 (1985).

[7]A. S. Barker, Jr. and M. Tinkham, J. Chem. Phys. **38**, 2257 (1963); W. G. Spitzer, R. C. Miller, D. A. Kleinman, and L. E. Howarth, Phys. Rev. **126**, 1710 (1962); S. D. S. Porto, P. A. Fleury, and T. C. Damen, *ibid.* **154**, 522 (1967).

[8]S. Shin *et al.*, Phys. Rev. B **41**, 4993 (1990).

[9]G. A. Samara and P. S. Peercy, Phys. Rev. B **7**, 1131 (1973), and references therein.

[10]M. H. Manghnami, J. Geophys. Res. **74**, 4317 (1969); J. Reintjes and M. B. Schulz, J. Appl. Phys. **39**, 5254 (1968).

[11]See, for example, N. F. Mott, *Metal-Insulator Transition* (Taylor & Francis, London, 1974), and references therein.

[12]R. F. Bongers, Solid State Commun. **3**, 275 (1965); I. Kitahiro, A. Watanabe, and H. Sasaki, J. Phys. Soc. Jpn. **21**, 196 (1966).

[13]S. C. Abrahams, Phys. Rev. **130**, 2230 (1963); F. J. Morin, Phys. Rev. Lett. **3**, 34 (1959).

[14]S. M. Shapiro, J. D. Axe, G. Shirane, and P. M. Raccah, Solid State Commun. **15**, 377 (1974); R. Pynn, J. D. Axe, and R. Thomas, Phys. Rev. B **13**, 2965 (1976).

[15]H. Terauchi and J. B. Cohen, Phys. Rev. B **17**, 2494 (1978); D. B. McWhan *et al.*, *ibid.* **10**, 490 (1974); G. Anderson, Acta Chem. Scand. **8**, 1599 (1954).

[16]D. Paquet and P. Leroux-Hugon, Phys. Rev. B **22**, 5284 (1980).

[17]E. N. Fuls, D. H. Hensler, and A. R. Ross, Appl. Phys. Lett. **10**, 199 (1967); G. A. Rozgonyi and D. H. Hensler, J. Vac. Sci. Technol. **5**, 194 (1968).

[18]C. H. Griffiths and H. K. Eastwood, J. Appl. Phys. **45**, 2201 (1974).

[19]E. E. Chain, J. Vac. Sci. Technol. A **4**, 432 (1986).

[20]F. C. Case, J. Vac. Sci. Technol. A **5**, 1762 (1987).

[21]G. A. Nyberg and R. A. Buhman, Thin Solid Films **147**, 111 (1987).

[22]E. Kazuno, J. A. Theil, and John A. Thornton, J. Vac. Sci. Technol. A **6**, 1663 (1988).

[23]H. L. M. Chang, H. You, J. C. Parker, J. Guo, Y. Gao, and D. J. Lam, in *High Performance Ceramic Films and Coatings*, edited by P. Vincenzini (Elsevier Science, New York, 1991), p. 161.

[24]H. L. M. Chang, H. You, J. Guo, and D. J. Lam, Appl. Surf. Sci. **48/49**, 12 (1991).

[25]H. L. M. Chang *et al.*, J. Mat. Res. **7**, 2495 (1991).

[26]H. You, H. L. M. Chang, R. P. Chiarello, and D. J. Lam, in *Heteroepitaxy of Dissimilar Materials*, edited by R. F. Farrow, MRS Symposia Proceedings No. 221 (Materials Research Society, Pittsburgh, 1991), p. 181.

[27]M. Born and E. Wolf, *Principles of Optics* (Pergamon, New York, 1959).

[28]B. E. Warren, *X-Ray Diffraction* (Addison-Wesley, Reading, MA, 1969).

[29]The scattering angle of sapphire $(11\bar{2}0)$ reflection is close to that of $(200)VO_2$ reflection and its higher harmonic occurs near the $(100)VO_2$ position.

[30]C. N. Berglund and H. J. Guggemheim, Phys. Rev. **185**, 1022 (1969).

[31]M. E. Fisher and A. N. Berker, Phys. Rev. B **26**, 2507 (1982).

[32]H. K. Kim, R. P. Chiarello, H. L. M. Chang, D. Lam, and H. You, in *Interface Dynamics and Growth*, edited by K. S. Liang, MRS Symposia Proceedings No. 237 (Materials Research Society, Pittsburgh, 1992), p. 417.

[33]M. S. S. Challa, D. P. Landau, and K. Binder, Phys. Rev. B **34**, 1841 (1986).

[34]J. Lee and J. M. Kosterlitz, Phys. Rev. B **43**, 3265 (1991).

[35]Kurt Binder, Rep. Prog. Phys. **50**, 783 (1987), and references therein.

[36]E. V. Babkin *et al.*, Thin Solid Films **150**, 15 (1987).